NASA CR- 112319
N73 25063

AUTOMATED DESIGN OPTIMIZATION OF SUPERSONIC AIRPLANE WING STRUCTURES UNDER DYNAMIC CONSTRAINTS

By Richard L. Fox, Hirokazu Miura, and Singiresu S. Rao

Prepared under Grant No. NGR 36-003-002 by
CASE WESTERN RESERVE UNIVERSITY
Cleveland, Ohio

for

NATIONAL AERONAUTICS AND SPACE ADMINISTRATION

AUTOMATED DESIGN OPTIMIZATION OF SUPERSONIC AIRPLANE WING STRUCTURES UNDER DYNAMIC CONSTRAINTS*

R. L. Fox
Associate Professor
Case Western Reserve University
Cleveland, Ohio

H. Miura
Research Associate
Technical University of Norway
Trondheim, Norway

S. S. Rao
Assistant Professor
Indian Institute of Technology
Kanpur, India

Abstract

The problems of the preliminary and first level detail design of supersonic aircraft wings are stated as mathematical programs and solved using automated optimum design techniques. The problem is approached in two phases: the first is a simplified equivalent plate model in which the envelope, plan form and structural parameters are varied to produce a design, the second is a finite element model with fixed configuration in which the material distribution is varied. Constraints include flutter, aeroelastically computed stresses and deflections, natural frequency and a variety of geometric limitations. The Phase I objective is a combination of weight and drag while Phase II is a weight minimization.

1. Introduction

This paper reports upon work which was undertaken to show the feasibility of automated design optimization of aircraft structures having practical scale and complexity and subject to involved dynamic behavior constraints. It should be viewed as a contribution to a long range effort to assemble an integrated capability for the computer aided design for aircraft. There are a number of large scale structural analysis programs in existence, but synthesis of a complicated system like an aircraft cannot be achieved practically at the present time by simply connecting such analysis programs together. Probably the best design system will be very flexible and versatile and hence will of necessity include human designers as an important element. We feel that such a system will be organized around a core of optimization methodology. Two hierarchial levels may be considered for this system: one is based on the substructuring of the physical airframe and its systems and the other is based on the level of idealization of each substructure and system and its interfaces with adjacent substructures or the environment.

The study reported herein has a position at a preliminary design stage and concerns the design of supersonic aircraft wings. It takes into account requirements on natural frequencies and flutter speed in addition to those on static behavior responses and geometric side constraints. It includes some examination of the consequences of changing the aerodynamic envelope as well as merely the structural contents of the wing. The motivation for including dynamic constraints in the preliminary design of aircraft wing structures is in the reported experiences of other investigators [1], in which significant modification of structures which were designed to satisfy static behavior constraints were required to meet requirements on dynamic behavior.

Structural optimization including dynamic constraints has been considered by many investigators. For multi-degree-of freedom structures, significant progress has been reported in recent years using the discrete methods of analysis, taking advantage, of course, of the capability of high speed digital computers. Among these, structural design for minimum weight subject to constraints on natural frequencies were reported by Turner [2], Zarghamee [3], Rubin [4], Fox and Kapoor [5], et al. In utilizing discrete methods, there is no theoretical difference between static and dynamic behavior constraints. However, practical and numerical difficulties do exist because dynamic analyses are usually time consuming and sensitivities of the behavior with respect to the change of design variables are difficult to obtain. The derivatives of natural frequencies with respect to design variables were presented in Refs. (3) and (5) and have been utilized in actual design procedures recently (3), (4), and (5). For the problem of structural optimization subject to flutter constraints, very little work has been done. Early work has been presented by Schmit and Thornton [6]. In their paper, a rectangular supersonic wing of symmetric double wedge profile was designed, subject to constraints on root angle of attack, tip deflection, stress at the root and flutter speed. Turner, in Ref. (7), [2] extended his previous work to the problem of attaining the minimum structural mass holding flutter speed constant. Simply supported panel (supersonic) and cantilever rectangular wing (subsonic) are considered as examples in this work. Very recently, Stroud et al [8] published work which is closely related to the work of this report. Their purpose is to obtain the optimal skin panel thickness distribution for minimum weight which satisfies both yield stress and flutter speed criteria for variable depth, clipped tip delta wing structures. Their structural model may be called a finite difference model, in which the spanwise displacement is considered at N stations parallel to the air stream and the chordwise displacement is approximated by a quadratic polynomial at each spanwise station.

* This work was supported in part by NASA under research grant NGR 36-003-002.

It is natural to desire to extend this trend and to establish some useful design procedures for practical wing structures. However, it is not realistic to take all requirements into account and analyze the structures in detail, even with the most advanced current computers. Consequently, in the study reported herein, the scope of the work is limited to the determination of the basic structural configuration and material distribution at the preliminary design stage of a new supersonic airplane.

The process involved in this study consists of two phases. The first is concerned with the determination of a simplified configuration of the wing structure and the aerodynamic envelope. In particular the simplified plan view shape of a low aspect ratio wing, the symmetric wing depth distribution and the cover panel thickness distribution are to be determined. The design process is constituted so that an objective function composed of the aerodynamic drag and the weight of the wing is minimized, subject to constraints on static and dynamic behavior for multiple flight and fuel conditions. The second phase is the determination of relatively detailed material distribution for a wing of fixed configuration. Here the wing is modeled with finite elements and the thicknesses of the cover plate elements, cross sectional areas of bar elements representing flanges, thickness of the webs of ribs and spars, and the magnitude of "tuning" masses are determined for minimum weight, subject to static and dynamic constraints for multiple flight conditions.

These two phases are independent and most of the analysis techniques are different. It is possible, however, tc accomplish an extensive preliminary design of a wing structure by using the results of these two studies sequentially. Namely, first determine the basic configuration and a very crude material distribution by using the routine developed in Phase I. Then using the optimal configuration, detailed material distribution is obtained by the Phase II routine.

2. Analytical Idealizations

2.1 Phase I

2.1.1 Structural Model

As an approximation, the wing of a supersonic aircraft may be regarded as a camberless, smooth, thin sandwich plate of variable thickness, and hence it is possible to consider this type of structure equivalently as a plate which has variable flexural rigidities and shear stiffness. This is called an "equivalent plate" model. A low aspect ratio wing may be composed of plate spars and ribs, and stiffened upper and lower cover panels. In Phase I, however, detailed structural arrangement and dimensions are not considered, and, therefore, such inhomogenieties of the core or the cover panels are smeared; i.e. the core is considered to be of a homogeneous, orthotropic material whose equivalent tensile and shear moduli are computed by smearing the material by the ratio of cross sectional areas, and the cover plates are also considered to be orthotropic plates of smooth thickness variation.

A wing is idealized as shown in Fig. 1, in which the plan view shape is a trapezoid defined completely by four parameters: R, S, θ_1, and θ_2.

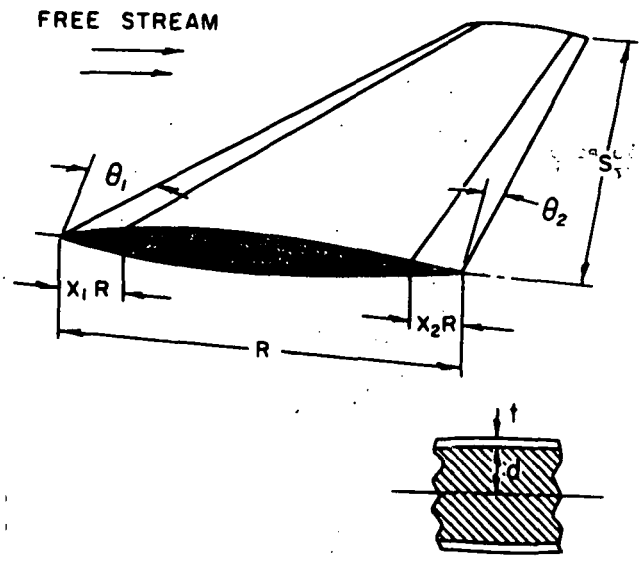

Figure 1

The wing depth distribution, d(x, y), and the cover panel thickness distribution, t(x, y), are expressed in the form of polynomials. These polynomials must be chosen so that a realistic and general distribution can be expressed with a minimum number of constants (design variables) and also d(x, y) must satisfy the condition of zero thickness at the leading and the trailing edges.

Our choices are:

$$d(x, y) = (\xi - \tan\theta_1 \frac{S}{L_x}\eta)(-\xi + \tan\theta_2 \frac{S}{L_x}\eta)(\frac{R}{L_x})(d_1 + d_2\xi + d_3\eta)$$

$$t(x, y) = (\xi - \tan\theta_1 \frac{S}{L_x}\eta)(-\xi + \tan\theta_2 \frac{S}{L_x}\eta)(\frac{R}{L_x})(t_1 + t_2\xi + t_3\eta) + t_0 \quad (1)$$

where

$$\xi = \frac{x}{L_x}$$

$$\eta = \frac{y}{L_y}$$

L_x, L_y : reference lengths

d_1, d_2, d_3 : wing depth design variables

t_1, t_2, t_3 : cover plate thickness design variables

t_0 : minimum gauge thickness of cover plates

For most airplane wings, certain portions near the leading and the trailing edges do not function as structural elements to carry bending and shear loadings: they may be control surfaces, lift augmentation devices or simply an extension of thin cover plates. To account for this effect, prespecified portions of the chord length from the leading and the trailing edges are excluded in computing stiffness characteristics of the wing structures.

A Ritz type displacement method is used to formulate the stiffness characteristics including transverse shear deformation. Basic assumptions employed in this process are:

(1) $t \ll d$
(2) In-plane displacement of the neutral surface is negligible.
(3) Young's modulus of the core in the transverse direction is infinitely large.
(4) The Love-Kirchoff hypothesis is valid throughout the core.

It was observed that the numerical accuracy of the computed behavior responses depends strongly on the choice of the assumed displacement functions. Sets of polynomials were determined so that each function is as strongly independent as possible from the others in the set. Ideally, these functions would be orthogonal but since this is a very difficult condition to meet in the odd shaped domain of the wing, a set which is "nearly" orthogonal in the wing domain was used. These consist of the following:

(1) Chordwise direction (Legendre Polynomials), defined in $0 \le \xi \le 1$

$$P_1(\xi) = 1$$
$$P_2(\xi) = 2\xi - 1$$
$$P_3(\xi) = 6\xi^2 - 6\xi + 1$$
$$P_4(\xi) = 20\xi^3 - 30\xi^2 + 12\xi - 1 \qquad (2)$$
$$P_5(\xi) = 70\xi^4 - 140\xi^3 + 90\xi^2 - 20\xi + 1$$
$$P_6(\xi) = 252\xi^5 - 630\xi^4 + 560\xi^3 - 210\xi^2 + 30\xi - 1$$

(2) Spanwise direction (see Ref. (9)), defined in $0 \le \eta \le 1$

$$H_1(\eta) = 1$$
$$H_2(\eta) = \eta$$
$$H_3(\eta) = \eta^2$$
$$H_4(\eta) = 6\eta^3 - 5\eta^2 \qquad (3)$$
$$H_5(\eta) = 28\eta^4 - 42\eta^3 + 15\eta^2$$
$$H_6(\eta) = 120\eta^5 - 252\eta^4 + 168\eta^3 - 35\eta^2$$
$$H_7(\eta) = 495\eta^6 - 1320\eta^5 + 1260\eta^4 - 504\eta^3 + 70\eta^2$$
$$H_8(\eta) = 2002\eta^7 - 6435\eta^6 + 7920\eta^5 - 4620\eta^4 + 1260\eta^3 - 126\eta^2$$

Using this set of polynomials, the transverse displacement $w(x, y)$, and the rotational angles of the midsurface in the x and y directions, $\alpha(x, y)$ and $\beta(x, y)$, respectively, are expressed as follows:

$$w(x, y) = \sum_{i=1}^{NX} \sum_{j=3}^{NY} w_{ij} P_i(\xi) H_j(\eta) \equiv \sum_{k=1}^{NW} W_k \phi_k(\xi, \eta) \qquad (4)$$

$$\alpha(x, y) = \sum_{i=1}^{NX-1} \sum_{j=1}^{NY} a_{ij} P_i(\xi) H_j(\eta) \equiv \sum_{k=1}^{NA} A_k \phi_k(\xi, \eta) \qquad (5)$$

$$\beta(x, y) = \sum_{i=1}^{NX} \sum_{j=1}^{NY-L} b_{ij} P_i(\xi) H_j(\eta) \equiv \sum_{k=1}^{NB} B_k \phi_{Bk}(\xi, \eta) \qquad (6)$$

where

NX, NY : numbers of displacement expansion functions used in the chordwise and the spanwise directions, respectively.

W_k, A_k, B_k : displacement degrees of freedom.

$$NW = NX \times (NY - 2)$$
$$NA = (NX - 1) \times NY$$
$$NB = NX \times (NY - 1)$$

Note that this chosen displacement pattern satisfies the following boundary conditions at the wing root.

$$w(x, 0) = 0$$
$$\frac{\partial w}{\partial y}(x, 0) = 0$$

Assemblage of the stiffness matrix is a straight forward procedure (see Ref. (9)), however, computationally, it takes a significant amount of time to build each new stiffness matrix.

2.1.2 Inertia Model

The structural mass densities of the core and the cover plate materials are considered to be uniform, i.e. inhomogenieties are smeared as was done for stiffness characteristics. It is found

in practice that considerable mass gets added in the form of stiffners, rivets, fillets, etc. to the "pure" structural parts in the actual structure. To account for this, the densities of the structural materials are taken as twice the actual material densities. Fuel stored in the wing is also considered to be distributed uniformly in the core and the total amount of fuel in the wing can be designated arbitrarily. Large concentrated masses such as engines are included as point masses at specified locations in the neutral plane of the wing.

Kinetic energy due to rotational motion is assumed to be negligibly small compared with that due to the transverse motion. The well known procedures for assembling the so called "consistent mass matrix" are used.[11]

2.1.3 Aerodynamic Model

Second order piston theory[12], in which the wing depth distribution is taken into account, is used to predict both the steady and unsteady pressure distributions on the wing surfaces. This theory is reasonably accurate for an air stream with Mach numbers greater than 2. For a wing of finite length, it is known that the pressure distribution on the surfaces which are inside the Mach comes induced at the tip or at the root is somewhat different from the one predicted by piston theory. No modification is made to account for this in the present study because of the need for simplicity of the analysis in this preliminary design optimization. For more rigorous analyses, the Mach box method, as was used by Giles[13] for supersonic wing structural design, may be an adequate choice for steady aerodynamics.

Applying piston theory, the local pressure acting on the midsurface is expressed[14]

$$\Delta P(x, y) = F_1(\xi, \eta, M_\infty)(\alpha_0 - \frac{\partial w}{\partial x}) - F_2(\xi, \eta, M_\infty)\frac{\partial w}{\partial t} \quad (7)$$

where

$$F_1(\xi, \eta, M_\infty) = 2\gamma M_\infty P_\infty (1 + \frac{\gamma + 1}{2} M_\infty \frac{\partial z}{\partial x})$$

$$F_2(\xi, \eta, M_\infty) = \frac{2\gamma}{a_\infty} P_\infty (1 + \frac{\gamma + 1}{2} M_\infty \frac{\partial z}{\partial x})$$

z : half of the wing depth at (x, y)

α_0: root angle of attack

Using Eq. (7), the work-equivalent load vector Q_A, associated with the transverse displacement vector, W, is expressed[9]:

$$\vec{Q}_A = \vec{Q}_{SA} - (A_1 + A_2)\vec{W} - (B_1 + B_2)\dot{\vec{W}} \quad (8)$$

where

$$Q_{SA} = \iint F_1(\xi, \eta, M_\infty)\alpha_0 \bar{\Phi}(\xi, \eta)dxdy$$

$$A_1 = 2\gamma M_\infty P_\infty \iint \bar{\Phi}(\xi, \eta) \frac{\partial \bar{\Phi}^T}{\partial x}(\xi, \eta)dxdy$$

$$A_2 = \gamma(\gamma + 1)M_\infty^2 P_\infty \iint \frac{\partial d}{\partial x} \bar{\Phi}(\xi, \eta) \frac{\partial \bar{\Phi}^T(\xi, \eta)}{\partial x} dxdy$$

$$B_1 = \frac{2\gamma}{a_\infty} P_\infty \iint \bar{\Phi}(\xi, \eta)\bar{\Phi}^T(\xi, \eta)dxdy$$

$$B_2 = \frac{\gamma(\gamma + 1)}{a_\infty} P_\infty M_\infty \iint \frac{\partial d}{\partial x}\bar{\Phi}(\xi, \eta)\bar{\Phi}^T(\xi, \eta)dxdy$$

A_1 and A_2 are unsymmetric "aerodynamic stiffness" matrices and B_1 and B_2 are symmetric aerodynamic "damping" matrices.

2.2 Phase II

2.2.1 Structural Model

The finite element method is used in the Phase II capability to represent the structural characteristics of the wing. It consists of representing a structural system as an assembly of elements as shown in Fig. 2. The nature of the multiweb

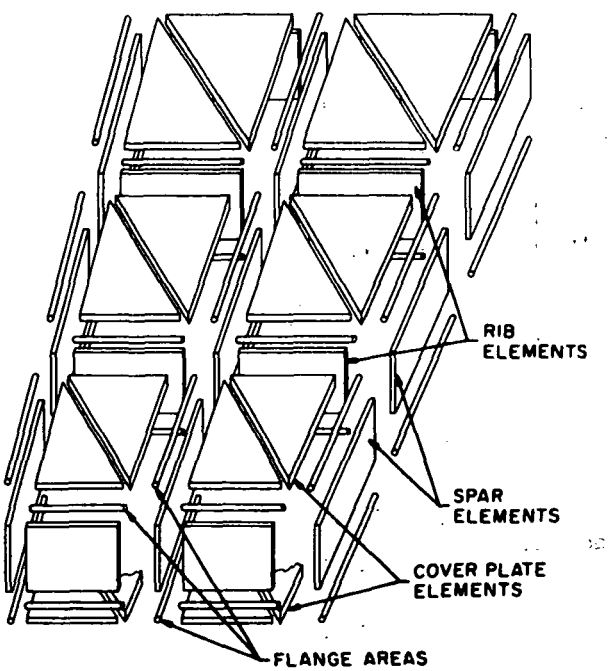

Figure 2

wing structure requires two distinct types of elements; one mainly to represent the wing cover panels which carry direct stress, and the other to represent the internal members which are effective in shear. If the direct stress carrying capability of the stringers are to be represented separately, a third kind of element is necessary to represent the stringers.

Previous studies by Gallagher, Rattinger and Archer [15], Tinawi [16], and Flemming [17] indicated that the static behavior of a wing structure is predominantly influenced by the choice of internal element (web) idealization, and not particularly by the idealization used for the skin panels. A comparative study of displacement and eigenvalue results was made to find the rates of convergence and the accuracies obtainable from different finite element idealizations (see Ref. (10)).

An idealization consisting of a combination of triangular membrane elements (cover panels), rectangular shear panels (webs) and pin-jointed bars (stringers or flanges) were found to be simple and accurate for representing the behavior of multiweb wing structures.

The procedure for assembling a stiffness matrix from such elements is well known and need not be discussed here.

2.2.2 Inertia Model

The consistent mass matrix was utilized for all structural elements, taking the densities of the structural materials as twice that of the real materials for the reasons discussed earlier. All nonstructural masses, such as fuel, engines and tuning masses, are considered to be concentrated at the nodes and therefore only influence the diagonal elements of the mass matrix.

The tuning masses are included for the purpose of suppressing flutter and have no load carrying capability as structural members.

2.2.3 Aerodynamic Model

The aerodynamic matrices are obtained by carrying out the surface integrals for all the cover plate elements using the expression for the pressure difference given by Eq. (7). The element air force matrices are obtained with respect to the local coordinate system and transformed into the global coordinate system.

3. Behavior Analysis and Design

In this section, the word "design" is taken to mean the determination of a set of values for the design variables so that a certain criterion value is optimized (minimized or maximized), while satisfying all constraints imposed on the behavior responses and dimensions of the structural system under consideration. This problem is formulated as a mathematical programming problem in the general form:

$$\text{Minimize } f(\vec{X})$$

$$\text{Subject to } g_j(\vec{X}) \le 0, \quad j = 1, 2, \ldots, NC \tag{9}$$

where

$\vec{X}$ is the vector of design variables,

$f(\vec{X})$ is a scalar function of $\vec{X}$: the objective function,

$g_j(\vec{X})$ is a scalar function of $\vec{X}$: a constraint function.

If this problem is to be solved automatically on a computer, repeated analyses of the responses of the system will be required corresponding to the sequential modifications of the design variables. Therefore, a next level of idealization or approximation is often useful in order to expedite the analyses of various behavior responses and their sensitivity to the change of design variables. Furthermore, efficiency of the design procedure is of critical importance in problems of this scale and complexity and only by taking advantage of the special structure and characteristics of the particular problems, can design be completed within acceptable computation time. The choice of algorithm and its modification to account for special features of given problems have a great deal of effect on the efficiency of the design process.

3.1 Phase I

3.1.1 Analyses of Behavior Responses

A complete equation of motion for the model described in the previous section can be written in a matrix form,

$$\begin{bmatrix} 0 \\ 0 \\ \ddot{M}\vec{W} \end{bmatrix} + \begin{bmatrix} 0 \\ 0 \\ (B_1+B_2)\dot{\vec{W}} \end{bmatrix} + (1 + ig_f) \times$$

$$\begin{bmatrix} K_{AA} & K_{AB} & K_{AW} \\ K_{BA} & K_{BB} & K_{BW} \\ K_{WA} & K_{WB} & (A_1+A_2+K_{WW}) \end{bmatrix} \begin{bmatrix} \vec{A} \\ \vec{B} \\ \vec{W} \end{bmatrix} = \begin{bmatrix} 0 \\ 0 \\ (\vec{Q}_W+\vec{Q}_{SA}) \end{bmatrix} \tag{10}$$

where

$\vec{W}$, $\vec{A}$, $\vec{B}$: vectors of displacement degrees of freedom

M: consistent mass matrix

K_{AA}, etc: partitioned elements of the stiffness matrix

$\vec{Q}_W$: static inertia load vector

$\vec{Q}_{SA}$: static aerodynamic load vector

g_f: structural damping coefficient

Equation (10) can be reduced to a smaller system by eliminating $\vec{A}$ and $\vec{B}$, if their values are not required explicitly.

$$M\ddot{\vec{W}} + [B_1 + B_2]\dot{\vec{W}} + [(1 + ig_f)K_R + A_1 + A_2]\vec{W} = \vec{Q}_W + \vec{Q}_{SA} \tag{11}$$

where

$$K_R = K_{WW} - [K_{WA} \quad K_{WB}] \begin{bmatrix} K_{AA} & K_{AB} \\ K_{BA} & K_{BA} \end{bmatrix}^{-1} \begin{bmatrix} K_{AW} \\ K_{BW} \end{bmatrix}$$

Throughout this study, the combination of NX = 3 and NY = 5 is used (where it will be recalled that NX and NY are the maximum numbers of displacement expansion functions in the chordwise and spanwise directions respectively). Thus the size of the system of Eq. (10) is 31 while that of Eq. (11) is only 9.

The governing equations for static equilibrium, natural vibration and flutter can be derived from Eq. (11) as follows:

Static Equilibrium: $\ddot{\vec{W}} = \dot{\vec{W}} = 0$, $g_f = 0$

$$[K_R + A_1 + A_2]\vec{W}_S = \vec{Q}_W + \vec{Q}_{SA} \tag{12}$$

Natural Vibration in Vacuum: $B_1 = B_2 = A_1 = A_2 = 0$

$$\vec{Q}_W = \vec{Q}_{SA} = 0 \ , \ g_f = 0$$

Assume: $\vec{W} = \vec{W}_v = \vec{W}_v e^{i\omega t}$

$$[-\omega^2 M + K_R]\vec{W}_r = 0 \tag{13}$$

Flutter: Assume $W = W_s + W_f e^{i\omega_f t}$

$$[-\omega_f^2 M + (1 + ig_f)K_R + A_1 + A_2 + i\omega_f(B_1 + B_2)]\vec{W}_f = 0 \tag{14}$$

The static displacement state can be computed by solving Eq. (12) for $\vec{W}_s$. Modification of the reduced stiffness matrix K_R by the aerodynamic stiffness matrices A_1 and A_2 eliminates the necessity of iteration on the displacement state and the pressure distribution on the wing surface. Determination of the root angle of attack to provide specified lift requires an iteration process, for which convergence is assured provided the wing is statically stable. The stress state in the cover panels must be computed using the displacement state obtained by solving the original Eq. (10) because computation of the stress state involves the rotational displacement vectors $\vec{A}$ and $\vec{B}$ as well as the transverse displacement vector $\vec{W}$.

The natural vibration frequencies are computed by solving a standard eigenvalue problem, Eq. (13), by Householder's method. To check the accuracy of the computed frequencies and mode shapes, flat plates of various plan view shape were analyzed and compared with experimental results given in the literature [9]. It was found that at least the three lowest natural frequencies were computed with reasonable accuracy.

The flutter condition is found as one of the solutions of a nonlinear, complex algebraic equation, Eq. (15), with respect to two unknowns,

$$|-\omega_f^2 M + (1 + ig_f)K_R + A_1 + A_2 + i\omega_f(B_1 + B_2)| = 0 \tag{15}$$

Among the NW solutions, the one which has the lowest Mach number gives the flutter condition. This is obtained in the Phase I capability by directly minimizing the absolute value of the flutter determinant in ω - M space by means of the conjugate gradient method [18]. Appropriate choice of an initial point for this minimization will assure convergence to a correct solution. Accuracy of this flutter analysis was studied by also comparing computed flutter conditions for flat plates of various plan view shapes and for a simply supported, infinitely long panel with theoretical and computed results given in the literature. It was found that the flutter Mach number is more sensitive than frequency to changes in the design variables, but satisfactory coincidence was observed as given in Ref. (9). It was also experienced that flutter conditions are associated with at least one bending mode and one twisting mode simultaneously, and that special care must be taken when the first twisting natural vibration mode shifts between the second and the third mode due to the changes of the design variables.

The aerodynamic drag acting on the wing may be separated into two parts. One corresponds to the resultant force component of air pressure acting on the wing surface in the direction of the free stream, and the other is due to the viscous friction between air and the solid wing surface. The former, pressure drag, can be computed by integrating the drag component of the local pressure over the entire wing surface.

$$D_p = 2M_\infty^2 P_\infty \iint [(\alpha_0 - w_x)^2 + d_x^2 - \frac{3}{4}\gamma(\gamma + 1)M_\infty^2(2\alpha_0 d_x w_x - d_x w_x^2)]dxdy \tag{16}$$

where

D_p : total pressure drag

w_x : $\frac{\partial w}{\partial x}$

d_x : $\frac{\partial d}{\partial x}$

The latter, friction drag, is computed by integrating the drag component of the friction stress over the entire wing surfact. The local friction stress distribution is obtained following the procedure given in Ref. (6), assuming that entire surface is covered by turbulent boundary layer.

$$\tau_F = \frac{0.259\ P_\infty M_\infty^2}{(1 + 0.13\ M_\infty^2)} \left\{ \log_{10} \frac{1.23\times10^7}{T_\infty^2(1 + 0.13M_\infty^2)^{5/2}} \times xP_\infty M_\infty[T_\infty(1 + 0.13M_\infty^2) + 198.7] \right\}^{-2.584} \tag{17}$$

The total friction drag D_F is,

$$D_F = \iint \tau_F[\cos(\alpha_0 - w_x + d_x) + \cos(\alpha_0 - w_x \pm d_x)]dxdy \quad (18)$$

3.1.2 Formulation of the Design Problem for Phase I'

Using the capability for analyzing the various behavior responses described previously, the design problem can be placed in the form given in Eq. (9).

The objective function for Phase I is chosen as a function of the structural weight of the wing and the aerodynamic drag, with the form of the function being arbitrary. The behavior constraints must be considered for every combination of the flight and fuel conditions. Two parametric* constraints, namely the stress and the displacement constraints, are simplified by choosing appropriate points where the most critical responses are expected.

Behavior Constraints

Stress: At five equally spaced points along the root, the Von Mises combined stress in the skin panel is computed, and it must not exceed the allowable level at any of the five points.

Displacement: Displacement of the leading and the trailing edges at the tip of the wing are computed, and neither of them may exceed the specified value.

Root Angle of Attack: The root angle of attack must be smaller than the specified value.

Gross Lift: The gross lift provided by the wing must be equal to the preassigned value. This equality constraint is incorporated in the computation of the root angle of attack and not treated as a separate constraint in the mathematical programming problem.

Natural Frequency: The fundamental frequency of natural vibration in a vacuum must be higher than the specified value. This constraint is independent of flight conditions.

Flutter Speed: The flutter Mach number must be higher than the flight Mach number multiplied by a safety factor.

Several geometrical side constraints are required to impose various restrictions of engineering significance.

Side Constraints

Plan View Shape: Upper limits are imposed on the root chord, lower limit on the semi-span, positive leading edge sweep angle and upper and lower limit of the trailing edge sweep angle.

Wing Area: A minimum wing area is imposed.

Positive Tip Chord: A constraint to avoid negative tip chord is imposed.

Wing Depth: Constraints to avoid negative wing depth are imposed.

Minimum Gauge Thickness on Skin Panel Thickness: Constraints to assure the minimum gauge thickness of the skin panel are imposed.

3.1.3 Optimization Algorithm for Phase I

The critical factor in choosing an appropriate algorithm is, of course, the computation time required to complete a design. Most of the efficient methods of optimization utilize derivatives (with respect to the design variables) of the constraint and objective functions. In this work, the complexity of the analyses is so great that the gradient of the behavior constraints and of the objective function can only be computed by a finite difference method. This requires a large number of function evaluations. By comparing various currently available algorithms, Zoutendijk's method of feasible directions (See Ref. (19) or for computational detain (21)) was selected for Phase I. Since it is observed that most likely the optimal designs are simultaneously on several constraints, the optimization procedure is carried out by staying close to the constraint hypersurfaces to find the vertex where the minimum of the objective function is achieved.

An important feature of this algorithm is the direction finding process by which a redesign direction is determined. Given a feasible design vector X_k, a new design is obtained by the step:

$$\vec{X}_{k+1} = \vec{X}_k + \alpha \vec{S}_k$$

where the direction of redesign $\vec{S}_k$ is determined so that for some $\alpha > 0$, $\vec{X}_{k+1}$ will be a feasible design with an improved value of the objective. The active constraint set at a design point $\vec{X}_k$ is determined by the criterion

$$-W_{Aj} \le g_j(\vec{X}_k) \le 0 \quad , \quad \forall_j \in J$$

where W_{Aj} is a positive scalar which specifies the width of the active range of the j^{th} constraint. At the point $\vec{X}_k$, the direction vector, $\vec{S}_k$, by which the design is to be modified, is determined by solving a special linear programming problem,

Minimize β

Subject to: $\vec{S}^T \nabla g_j(\vec{X}_k) + \theta_j \beta \le 0 \quad , \forall_j \in J$

$\vec{S}^T \nabla f(\vec{X}_k) + \beta \le 0$

Norm of $\vec{S}$ is bounded

where θ_j are non-negative scalars that determine how far the vector $\vec{S}$ must be pushed into the

* Parametric constraints are those which must be satisfied for a range of some parameter or parameters: in this case, x and y are parameters for the stress and displacement constraints.

feasible region in order to avoid violation of the same constraint due to its curvature. For example, if $\theta_j = 0$, $\vec{S}$ may be tangent to the hypersurface $g_j(\vec{X}) = 0$. If θ_j is positive, $\vec{S}$ must lie strictly inside a cone with its axis on the vector $-\nabla g_j(\vec{X}_k)$, with the apex on $\vec{X}_k$ and with the open angle determined by (but not equal to) θ_j. In this study, the value of θ_j is determined by the following relation

$$\theta_j = \frac{g_j(\vec{X}_k)}{W_{Aj}} + 1 \qquad (20)$$

This form is based on Vanderplaats' modification [20].

It is reported that the method of feasible directions may have slow convergence due to a behavior called zig-zagging [21]. For the purpose of avoiding this difficulty and also to improve the efficiency, the following schemes are employed in addition to the basic algorithm.

(1) If an active constraint $g_j(\vec{X}_k)$ is linear with respect to the design variables, θ_j is set to zero.

(2) If a nonlinear constraint becomes active successively, then θ_j for that constraint is increased by the following equation.

$$\theta_j = \frac{g_j(\vec{X}_k)}{W_{Aj}} + 1 + (NSH_j - 1)\varepsilon_T \qquad (21)$$

where NSH_j is the number of successive encounters of the same constraint, $g_j(X)$, and ε_T is a constant which is chosen to be 0.1 in this study.

(3) If a constraint $g_j(X)$ is encountered and alternatively becomes inactive and active more than three times, the constraint is always kept active until convergence is obtained. Then the normal optimization procedure is started again from that tentative optimal point.

(4) The active width of the constraints is taken to be large (for example, 5 ~ 10% of normalized values of the constraints) and if an optimum is achieved tentatively, then the active width of the constraints which are currently active is cut to smaller width and optimization is continued from the point achieved previously. If the current effective width of all constraints which are active at that tentative optimal point are smaller than the specified values, this sequence is stopped.

(5) Design variables are scaled so that the components of the gradient vectors have nearly the same order of magnitude. this will generally cause the direction finding procedure to be better conditioned. The scaling factors are determined as a result of a sensitivity analysis made at various points in the feasible region.

(6) The maximum step size is restricted because the starting point for the flutter analysis may be too far from the true flutter condition and cause numerical difficulties.

(7) Since computation of the flutter constraints is time consuming, none of flutter constraints are incorporated at the beginning. At the end of each one-dimensional minimization, all flutter constraints are checked and if new flutter constraints are violated, that stage of one dimensional minimization is repeated by taking the violated flutter constraint into account. This flutter constraint is then included in all following computations.

3.2 Phase II

3.2.1 Analyses of Behavior Responses

Using the finite element model described in Section 2.1, the stresses, displacements, natural vibration frequencies and flutter conditions are to be computed. The governing equations for these quantities are obtainable through standard procedures and details are presented in Ref. (10).

The static displacement state is obtained by solving the system of equations

$$K\vec{Y}_s = \vec{P} \qquad (22)$$

where K is the master stiffness matrix of the structure, and the vectors $\vec{Y}_s$ and $\vec{P}$ represent, respectively, the displacement and the load vectors. A clamped boundary condition is specified along the root of the wing, thereby neglecting any influence of the flexibility of the fuselage. In addition, the number of degrees of freedom involved in the static analysis is reduced to one half of the total degrees of freedom of the system by assuming the wing to by symmetric about its middle plane and by choosing the node points of the elements on the top and the bottom surfaces of the wing to be symmetric. Namely, the number of displacement variables are reduced by one half by making the following two assumptions:

(a) The vertical displacements of the upper and lower surface points at a given planform location are equal.

(b) The inplane displacements of these same respective points are equal and opposite.

Since the load vector $\vec{P}$ depends on the root angle of attack α_0 and the displacement state $\vec{Y}_s$, an iteration process is necessary to determine the root angle of attack which provides the specified gross lift. This is indicated in the flow diagram of Fig. 3. The stress state induced in the finite elements can be determined from the known nodal displacements $\vec{Y}_s$ by using the stress-strain and the strain-displacement relations of linear elasticity. The stress information is also used for the purpose of checking a simple form of local buckling of the stiffened cover plates

and/or face wrinkling of the sandwich panels.

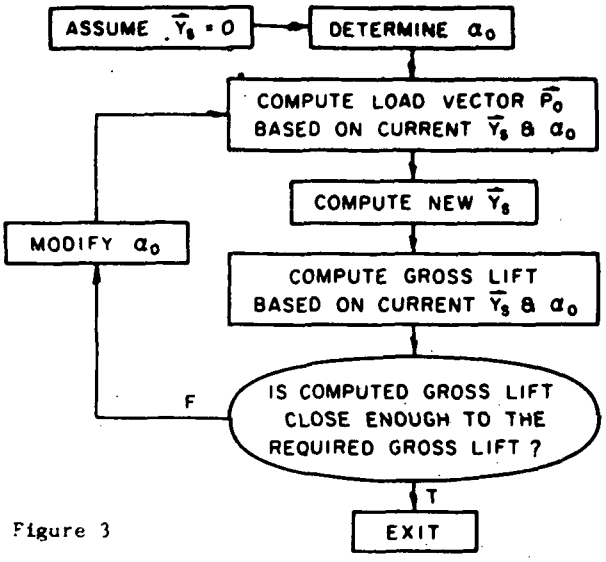

Figure 3

Frequencies of natural vibration in a vacuum are computed by solving an eigenvalue problem

$$[K - \omega^2 M]\vec{Y}_v = 0 \tag{23}$$

The determination of eigenvalues and eigenvectors is notoriously time consuming and it was therefore desirable to further reduce the degrees of freedom of the system so as to make the solution process more economical. The reduction technique used in the present study is similar to the one outlined in Ref. (22), namely, the elimination of coordinates at which the expected inertial forces can be assumed to be small. Accordingly, the degrees of freedom associated with the transverse displacements are retained by eliminating those corresponding to inplane displacements; this is in addition to the linking among coordinates used in the static analysis. The order of the eigenproblem is thus reduced to one-third that of the corresponding static problem. The reduction process is based upon the partition of Eq. 23, as follows

$$\begin{bmatrix} K_{11} & K_{12} \\ p\times p & p\times q \\ K_{21} & K_{22} \\ q\times p & q\times q \end{bmatrix} - \omega^2 \begin{bmatrix} M_{11} & M_{12} \\ M_{21} & M_{22} \end{bmatrix} \begin{bmatrix} \vec{Y}_{V_1} \\ \vec{Y}_{V_2} \end{bmatrix} = \begin{bmatrix} \vec{0} \\ \vec{0} \end{bmatrix} \tag{24}$$

It is assumed that the modes of natural vibration can be achieved sufficiently accurately by taking the vector $\vec{Y}_{V_2}$ to be related to $\vec{Y}_{V_1}$ as in a purely static problem. Consequently, Eq. (24) can be written in a reduced form

$$[K_r - \omega^2 M_r]\vec{Y}_{V_1} = 0 \tag{25}$$

where

$$K_r = [K_{11} - K_{12}K_{22}^{-1}K_{21}] \tag{26}$$
$p\times p$

$$M_r = [M_{11} - M_{12}K_{22}^{-1}K_{21} - K_{12}K_{22}^{-1}M_{21} + K_{12}K_{22}^{-1}M_{22}K_{22}^{-1}K_{21}] \tag{27}$$
$p\times p$

The reduced system, Eq. (25) is solved by using Choleski decomposition on M_r and Householder's method successively. To check the accuracy of the frequencies obtained from the reduced system, natural vibration frequencies of 60 d.o.f. (original) and 20 d.o.f. (reduced) system representing a cantilevered box beam were computed and compared. Eigenvalues associated with the transverse vibration agree well with differences less than 1% for all 18 modes [10].

The governing equation for flutter at neutral stability is expressed in a form

$$[K_r - \omega^2 M_r + Q_r]\vec{Y}_f = 0 \tag{28}$$

The aerodynamic matrix Q_r is assembled from element aerodynamic matrices Q^i, expressed as follows

$$Q^i = 2\rho_\infty a_\infty V_\infty A^i + i2\rho_\infty a_\infty \omega B^i + \rho_\infty(\gamma+1)V_\infty^2 C^i + i\rho_\infty(\gamma+1)V_\infty \omega D^i \tag{29}$$

where

ρ_∞ : Free stream mass density

V_∞ : Free stream air velocity

$$A^i = \iint \vec{a}^T \frac{\partial \vec{a}}{\partial x}\, dxdy$$

$$B^i = \iint \vec{a}^T \vec{a}\, dxdy$$

$$C^i = \iint \frac{\partial z}{\partial x} \vec{a}^T \frac{\partial \vec{a}^T}{\partial x}\, dxdy$$

$$D^i = \iint \frac{\partial z}{\partial x} \vec{a}^T \vec{a}\, dxdy$$

and $a^i(x, y)$ is a column vector of displacement interpolation functions of the i^{th} triangular membrane element for cover plates,

$$\vec{a}^i(x, y) = \frac{1}{2A^i_{123}} \begin{bmatrix} (y_3^i - y_2^i)(x - x_2^i) - (x_3^i - x_2^i)(y - y_2^i) \\ (y_1^i - y_3^i)(x - x_3^i) + (x_3^i - x_1^i)(y - y_3^i) \\ (y_2^i - y_1^i)(x - x_1^i) - (x_2^i - x_1^i)(y - y_1^i) \end{bmatrix} \tag{30}$$

where A^i_{123} is the area of the triangular element i.

After assembly, the aerodynamic matrix Q_r is arranged in the following form.

$$Q_r = 2\rho_\infty a_\infty V_\infty A_r + i2\rho_\infty a_\infty \omega B_r + \rho_\infty(\gamma+1)V_\infty^2 C_r + i\rho_\infty(\gamma+1)V_\infty \omega D_r \tag{31}$$

Suppose the flutter mode can be expressed by

$$\vec{Y}_{F_1} = \underset{p\times s}{U}\,\vec{\xi} \tag{32}$$

where the columns of U represent the s-lowest natural vibration modes and the complex vector $\vec{\xi}$ is a vector of model participation coefficients. By substituting Eq. (32) into Eq. (28) and premultiplying U^T, Eq. (32) is reduced to a smaller

(s×s) system.

$$\left\{ \begin{bmatrix} \omega_1^2 M_{11} & & \\ & \ddots & \\ & & \end{bmatrix} - \omega_i^2 \begin{bmatrix} M_{11} & & \\ & \ddots & \\ & & \end{bmatrix} + 2\rho_\infty a_\infty V_\infty \left([A] + \frac{\gamma+1}{2} \frac{V_\infty}{a_\infty} [C] \right) + i2\rho_\infty a_\infty \omega \left([B] + \frac{\gamma+1}{2} \frac{V_\infty}{a_\infty} [D] \right) \right\} \vec{\xi} = 0 \qquad (33)$$

The requirement for this equation to have a non-trivial solution is that both the real and imaginary parts of the coefficient determinant be zero. The two unknown parameters in this determinant are ω and V_∞ and the combination of (V_∞, ω) having the lowest V_∞ and that makes the determinant vanish is the flutter condition. This problem is solved by a double iteration process given in detail in Ref. (10).

The gradient of the behavior responses with respect to the design variables are obtained in various ways. The derivatives of the static responses are computed by finite difference and those for natural frequencies and Mach number are computed using analytical relations obtained by assuming that the mode shapes are independent of small changes in the design variables.

3.2.2 Formulation of the Design Problem for Phase II

The objective function used in Phase II is the structural weight of the wing. Multiple flight conditions and an arbitrary fuel condition and gross lift requirement can be specified. Two parametric constraints, viz. the stress and the displacement constraints, are simplified by choosing appropriate points or elements where the most critical responses are expected.

Behavior Constraints

Stress: For a preassigned set of cover plate elements near the root, normal stress components are computed, and they must not exceed specified values for these elements.

Cover Plate Local Buckling and Face Wrinkling: For a preassigned set of cover plate elements near the root, the compressive stress components in the spanwise direction are computed. These stress levels must not exceed the estimated buckling stress of the stiffened panel nor the estimated wrinkling stress of the sandwich plate. See Ref. (10).

Gross Lift: The gross lift provided by the wing must be equal to the given value for each flight condition. This equality constraint is incorporated in the computation of the static responses and is not treated as a constraint in the optimization problem.

Natural Frequencies: Preassigned number of natural frequencies may have the upper and lower bounds imposed for each fuel condition.

Flutter Speed: The flutter Mach number must be higher than the flight Mach number for each flight condition.

Side Constraints

The cover plate thicknesses have upper and lower bounds, the spar and the rib thickness have lower bounds, and the bar elements also have lower bounds. The tuning masses used for flutter suppression can have upper and lower bounds.

3.2.3 Optimization Algorithm for Phase II

In Phase II, the sequential unconstrained minimization technique (SUMT) is used by transforming the constrained problem into an unconstrained problem through an interior penalty function formulation. Primary reasons for this choice are

(1) The algorithm for the unconstrained minimization of arbitrary functions are well studied and generally are reliable.

(2) The penalty function methods allow the use of approximate analyses, at least, during the early stage of optimization.

(3) The variable metric unconstrained minimization technique used for the direction finding process is inherently stable and little affected by minor errors introduced through the analysis approximation.

The general problem, Eq. (9), is transformed into the problem,

Minimize:

$$\phi(\vec{X}, r_k) = f(\vec{X}) - r_k \sum_{j=1}^{NC} \frac{1}{g_j(\vec{X})} \qquad (34)$$

Starting from a feasible point, $\vec{X}_0$, the function $(\vec{X}, r_k)$ is minimized for a decreasing sequence of positive real numbers, r_k.

For a minimization procedure, the Davidon-Fletcher-Powell variable metric method [23] is used. This is considered to be the most powerful general algorithm known to date for finding an unconstrained local minimum of a function of many variables. The i^{th} direction vector $\vec{S}_i$ is found as

$$\vec{S}_i = - H_i \nabla\phi(\vec{X}_i) \qquad (35)$$

where the matrix H_i is updated by

$$H_{i+1} = H_i + \frac{\alpha^* \vec{S}_i \vec{S}_i^T}{\vec{S}_i^T \vec{V}_i} + \frac{H_i \vec{V}_i \vec{V}_i^T H_i^T}{\vec{V}_i^T H_i \vec{V}_i}$$

$$\vec{V}_i = \nabla\phi(\vec{X}_{i+1}) - \nabla\phi(\vec{X}_i) \qquad (36)$$

$$H_0 = I$$

The one dimensional search problem is to find $\alpha = \alpha^*$ which yield the first local minimum of

$$\phi(\vec{X}_i + \alpha\vec{S}_i, r) \equiv \phi(\alpha) \qquad (37)$$

An efficient one-dimensional search method developed by Lasdon, Fox and Ratner [25] is used in this study. This process consists of three stages: a linear, a quadratic, and a cubic approximation. The function values and first derivatives of $f(\vec{X})$ and $g_i(\vec{X})$ are used systematically in the three stages to locate the minimum with a restricted number of function evaluations.

Several important features utilized in this optimization algorithm are the following:

(1) The initial value of r_k (i.e. r_1) is chosen so that it satisfies

$$1.25f(\vec{X}_0) \le \phi(\vec{X}_0, r_1) \le 2.0f(\vec{X}_0)$$

and the values of r_{k+1} are found by using the relation

$$r_{k+1} = 0.1\ r_k.$$

(2) The criterion for termination of minimization for each r_k is provided by the following relation

$$\frac{\nabla\phi_i^T H_i \nabla\phi_i}{2\phi_i} = \frac{\vec{S}_i^T \nabla\phi_i}{2\phi_i} < \varepsilon$$

(3) The criterion for termination of the entire optimization is provided by the Kuhn-Tucker conditions: i.e. that the computed Lagrange multipliers for the active constraints are all negative.

(4) A certain amount of interaction between the operator of the program and the computer itself were found to be useful in saving computer time. Up to 40% of the computer time can be saved by adjusting the convergence criteria.

4. ILLUSTRATIVE EXAMPLES

Because of the complexity of the problem, it requires a large amount of data to present complete information to make the results reproducible. The data presented in this section are therefore only summaries which should be sufficient to visualize the problems and the significance of the optimization results. For more complete data, the principal references (9) and (10) should be consulted.

Cases 1, 2 and 3 are examples for Phase I and Cases 4, 5 and 6 are examples for Phase II. Cases 3 and 6 are sequential as described in Section 1. The important design conditions for all cases are given in Table 1.

Cases 1 and 2

These two cases use only different objective functions and demonstrate the effects of this choice on the optimal designs. In Case 1, the aerodynamic drag (in pounds) is considered to be 10 times more important than the weight of the wing (in pounds). Drag is computed in flight condition 1 with a vertical acceleration of 1 g. As shown in Table 2, the wing depth is decreased by 44.6% at the root, while the skin panel thinkness is increased by 98.1%, thus the resultant weight is increased by 26.8%. But the objective function decrease of 27.5% is achieved due to large reduction in both friction and pressure drag (see Fig. 5). In Case 2, the aerodynamic drag and the weight are considered to be equally important. Consequently, as shown in Table 2, the cover panel thickness is decreased by 48.6%. The increase in pressure drag is induced by a twisting deflection (leading edge up) due to the

TABLE 1 DESIGN CONDITIONS

	Cases 1 & 2		Case 3		Case 4		Case 5		Case 6	
Flight Conditions	1	2	1	2	1	2	1	2	1	2
Altitude	40,000 ft.	60,000	25,000	35,000	25,000	35,000	30,000	40,000	25,000	35,000
Flight Mach Number	3.0	2.2	2.5	3.5	2.5	3.5	2.6	3.0	2.5	3.5
Speed of Sound	11,660 in/s	13,660.0	12,193.0	11,678.0	12,193.0	11,678.0	11,938.8	11,617.2	12,193.0	11,678.0
Air Density	2.83×10^{-8}	1.09×10^{-8}	5.14×10^{-8}	3.56×10^{-8}	5.14×10^{-8}	3.56×10^{-8}	4.30×10^{-8}	2.83×10^{-8}	5.14×10^{-8}	3.56×10^{-8}
Vertical Acceleration	2.5 (up)	2.5 (up)	3.5	3.5	3.5	3.5	3.0	3.25	3.5	3.5
Fuel	0.645×10^{-4} (density) lb-s^2/in		0.645×10^{-4} (density)		243,000 b.	220,500 lb.	159,000 lb.	143,100 lb.	0	200,000 lb
Engines	77.2 lb-s^2/in		121.0 lb-s^2/in		113.0 lb-s^2/in		62.1 lb-s^2/in		121.0 lb-s^2/in	
Material	Cover	Core	Cover	Core						
Young's Modulus E_x	1.06×10^7 psi	7.06×10^3	1.64×10^7	9.65×10^3	(Isotropic)		(Isotropic)		(Isotropic)	
E_y	1.06×10^7 psi	1.04×10^6	1.64×10^7	9.65×10^3	$E = 1.64\times10^7$		$E = 1.64\times10^7$		$E = 1.64\times10^7$	
Shear Modulus G_{xy}	4.0×10^6 psi	0	0.63×10^7	0	$\nu = 0.3$		$\nu = 0.3$		$\nu = 0.3$	
G_{xz}	4.0×10^6 psi	2.66×10^3	0.63×10^7	3.71×10^3						
G_{yz}	4.0×10^6 psi	5.32×10^3	0.63×10^7	3.71×10^3						
Poisson's Ratio ν_{xy}	0.3	0	0.3	0						
ν_{yz}	0.3	0	0.3	0						
Density	2.485×10^{-4} lb-s^2/in^4	0.497×10^{-6}	4.145×10^{-4}	2.445×10^{-7}	4.145×10^{-4}		4.145×10^4		4.145×10^{-4}	
Material	Aluminum Alloy	Aluminum Alloy Grid	Titanium	Titanium Grid	Titanium		Titanium Sandwich		Titanium	
Objective Function	Case 1: drg + 0.1 wt.	Case 2: drg + wt.	drg + 0.1 wt.		weight		weight		weight	
Safety Factors										
Vertical Acceleration	1.5		1.0		1.0		1.0		1.0	
Flutter Speed	1.4		1.25		1.0		1.0		1.25	

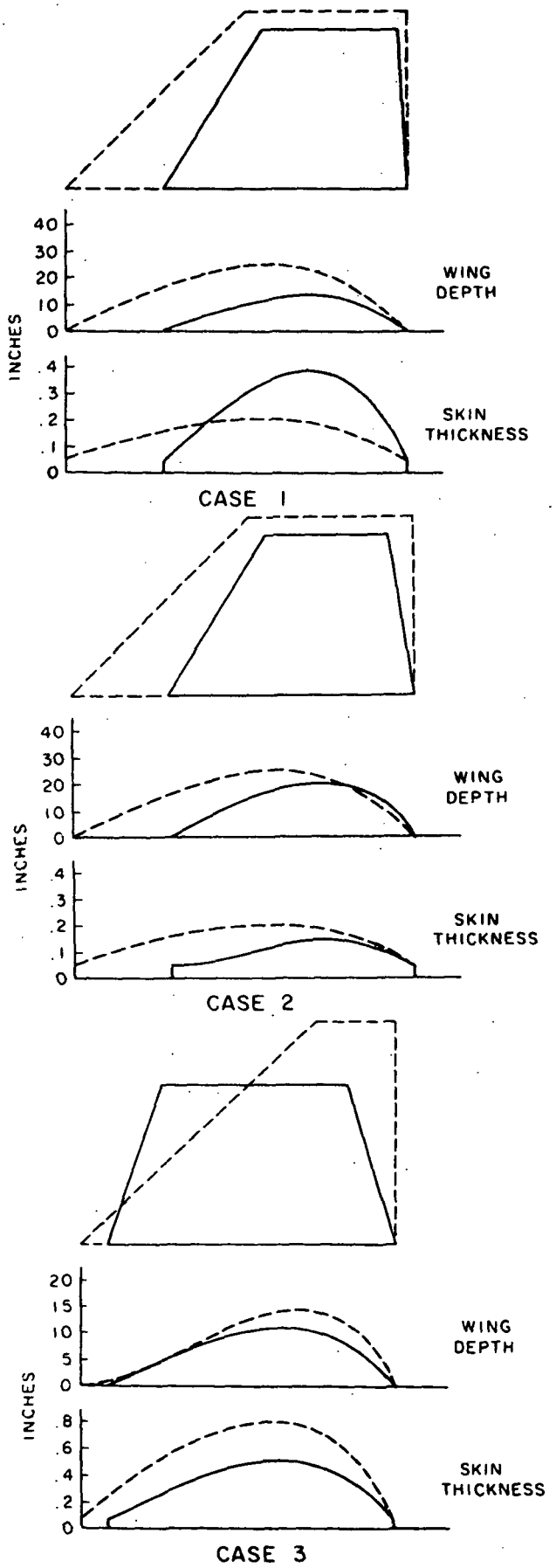

Figure 4

decrease of the stiffness. Simple presentations of these results are given in Fig. 4.

For these examples, the plan view shapes are restricted primarily by the minimum semi-span constraint. If stricter angle of attack or wing area constraints are imposed, the wing shape becomes stretched in the chordwise direction and the root chord constraint becomes a binding constraint (9).

Case 3

This case shows an example for a larger titanium wing. By relaxing the trailing edge sweep angle constraint, an almost symmetric plan view configuration is achieved. In the course of the optimization process, a natural vibration mode shift is observed. At the initial design, the first and the second natural vibration modes are associated with bending and the third mode is associated with twisting and the flutter frequency is between the second the the third natural frequencies. After four iterations, however, the twisting mode is shifted to the second mode and the true flutter frequency is found between the first and the second natural vibration frequencies.

When this type of mode shift happens, it is often the case that the initial point of flutter condition search becomes inadequate and the design process must be stopped and restarted manually. If this occurs near the optimum, accurate and stable flutter condition search may become difficult Simple presentation of this optimization result is given in Fig. 4.

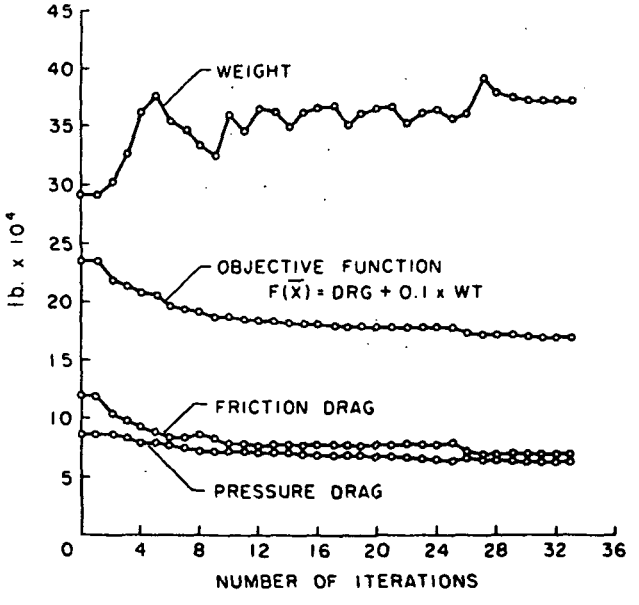

Figure 5

Cases 4(a) and 4(b)

The wing shown in Fig. 6 is considered. It has a 45° leading edge sweep angle and a planform area of 4,460 sq. ft. The material is Titanium. The thicknesses of the triangular elements marked "1" in the figure are taken as design variable x_1; the thicknesses of the other skin elements are taken as x_2. The variables x_3 and x_4 correspond to the rib and spar web thicknesses respectively and the flange areas of the ribs and spars are taken as x_5 and x_6 respectively. The four tuning masses are x_7, x_8, x_9, and x_{10}.

The difference between Cases 4(a) and 4(b) is merely the convergence criterion in the optimization procedure. In Case 4(a), a tight criterion was used to terminate the minimization for each r value while in Case 4(b), more relaxed criteria were used. Figure 7 shows the penalty function of 4(a) vs. the number of minimization steps and the objective functions of 4(a) and 4(b). The objective function has been scaled before incorporation into the penalty function. The differences in the optimal designs are interesting but the near equality of the objective functions merely indicates that the optimal region may be relatively flat in this problem. The flutter speed at low altitude is the active constraint and the tip displacement at high altitude is approaching an active status. These results are presented in Table 3.

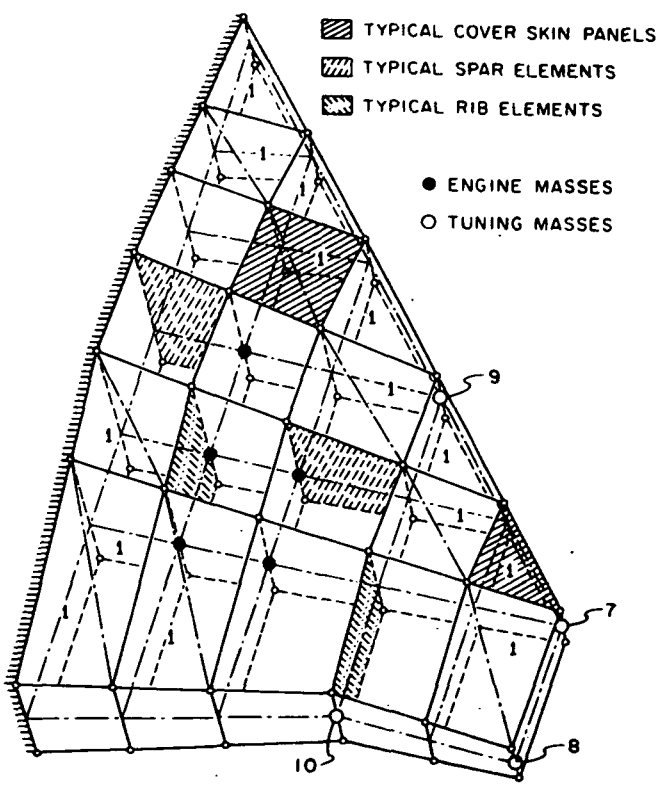

Figure 6

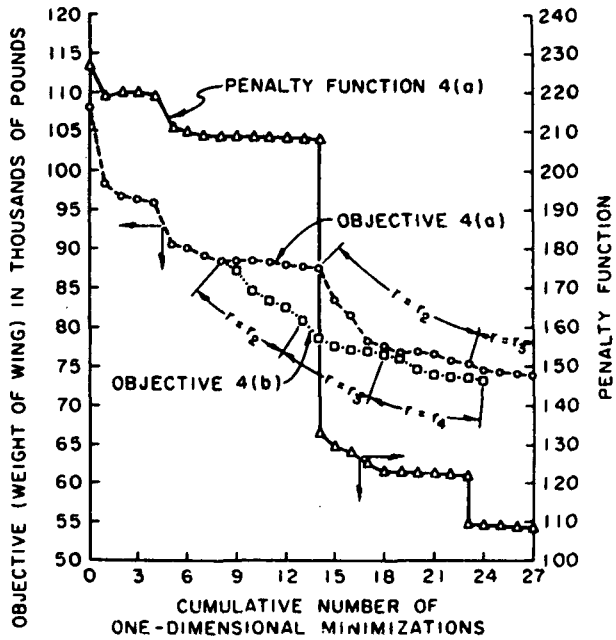

Figure 7

Case 5

This case is a delta wing with the skin design variables x_1, x_2 and x_3; rib and spar web variables x_4 and x_5; rib and spar flange variables x_6 and x_7; and tuning masses x_8, x_9 and x_{10}. The active constraints at the optimum are the flutter Mach number, the tip displacements, the face wrinkling stress, and a natural frequency limit. In addition x_1, x_5, x_8, x_9, and x_{10} are at their lower limits.

Case 6

The wing configuration and depth distribution from Case 3 (a Phase I example) were used to generate a finite element model. The design conditions were generally the same although there are some necessary changes in detail. Basically what we have is an attempt to design a more detailed version of the wing "predicted" as the optimal by Phase I. The results at first seem disappointing in that no improvement is possible over the initial design. In fact, a number of optimization runs produced several designs which differed a little in detail, but which were all within a few percent of the initial design in weight. The reason for this is that the initial design (given in Table 3) is derived from the optimal results of Case 3. To the extent that the analyses are comparable, the same constraints are active in both cases.

It is encouraging, in fact, that the Phase II program is essentially satisfied with the output of Phase I. On the other hand in other cases where a distribution of structural material which is substantially different from the uniform one of the Phase I model is better, the Phase II program will obtain it.

TABLE 2 RESULTS OF OPTIMIZATION

		Case 1		Case 2		Case 3	
		Initial	Optimal	Initial	Optimal	Initial	Optimal
Design Variables							
Root Chord	(in)	1250.0	905.73		854.26	1150.0	1121.1
Semi-span	(in)	650.0	600.03(a)		600.03(a)	850.0	600.0(a)
Leading Edge Sweep	(deg)	45.0	30.93		29.6	45.0	21.3
Trailing Edge Sweep	(deg)	0.0	-1.10	Same as Case 1	-10.0(g)	0.0	-20.0(k)
Wing Depth d_1	(in)	80.0	28.60		58.05	0.0	6.62
d_2	(in)	50.0	34.27		53.06	100.0	55.13
d_3	(in)	0.0	9.15		27.53	100.0	41.16
Cover Panel Thickness t_1	(in)	0.4	0.6926		10^{-5} (h)	2.0	1.518
t_2	(in)	0.4	1.2328		0.5243	2.0	1.759
t_3	(in)	0.0	0.3816		0.4305	2.0	1.639
Objective Function	(lb)	23,408.6	17,005.5	49,987.1	34,722.1	94,342.8	53,445.4
Weight	(lb)	29,431.7	37,280.7		15,100.3	140,647.4	106,278.9
Pressure Drag	(lb)	8,545.3	6,400.6	Same as Case 1	13,906.4	49,890.1	18,539.0
Friction Drag	(lb)	11,920.2	6,878.9		5,715.9	30,388.1	24,278.5
Representative Constraints							
Wing Area	(in^3)	4,180.0	2,275.0	Same as Case 1	2,140.0	4,280.0	3,310.0
Flutter Mach No. no fuel F. C. 1	(f)	7.30	6.77		6.59	6.09	3.35
Flutter Mach No. no fuel F. C. 2		3.28	3.08(b)		3.13(b)	8.66	4.94
Flutter Mach No. full fuel F. C. 1		9.00	7.42	Same as Case 1	8.30	8.00	3.17(c)
Flutter Mach No. full fuel F. C. 2		4.15	3.34		4.14	10.9	4.72
Ang. Attack, full fuel F.C.2	(deg)	6.5	8.85		9.98(f)	5.60	5.35
Stress full fuel F.C.1	(ksi)	4.47	19.97(d)	Same as Case 1	19.63(d)	19.07	97.15(e)
Stress full fuel F.C.2	(ksi)	4.30	19.49(d)		19.10(d)	19.28	100.00(e)

Active and near Active Constraints

(a) Lower Bound = 600.0, (b) Lower Bound = 3.08, (c) Lower Bound = 3.125, (d) Upper Bound = 20, (e) Upper Bound = 100, (f) Upper Bound = 10°, (g) Lower Bound = 10°, (h) Lower Bound = 0, (k) Upper Bound = 20°, (f) Flight Condition

TABLE 3 RESULTS OF OPTIMIZATION

	Case 4*		(a)*	(b)*	Case 5+		Case 6
	Initial		Optimal	Optimal	Initial	Optimal	
Design Variables							
Cover plates t_1	.200	in.	.0845	.0829	.050	.0414(h)	0.25
t_2	.200	in.	.2086	.2107	.085	.0901	0.35
t_3	-		-	-	.095	.0839	0.35
Rib thickness T_1	.100	in.	.0859	.0685	.195	.1022(j)	0.25
Spar thickness T_2	.100	in.	.1280	.1548	.195	.1004(j)	0.25
Chordwise bars A_1	.250	$in.^2$	.1586	.0747	.200	.1025	0.25
Spanwise bars A_2	.250	$in.^2$	.1680	.0507(a)	.200	.1132	0.25
Tuning masses m_1	5000.0	lb	1051.0	757.0	1950.0	1008.0(c)	2500.0
m_2	5000.0	lb	1126.0	924.0	1950.0	1014.0(c)	2500.0
m_3	5000.0	lb	897.0(b)	674.0(b)	1950.0	1011.0(c)	-
m_4	5000.0	lb	964.0	683.0	-	-	-
Objective function	108,127	lb	74,380	73,258	30,486	22,769	106,500
Representative Constraints							
Tip defl. F.C.2	74.76	in	84.23(k)	84.31(k)	58.96	61.86(e)	69.0
Root stress F.C.2	54.47	ksi	60.66	60.88	75.02	76.25	57.0
Skin buckling F.C.2	52.57	ksi	67.06	67.48	72.52	74.61	41.6
Face Wrinking str. F.C.2	-		-	-	72.52	74.61(f)	-
Flutter Mach No. F.C.1	3.04		2.51(d)	2.51(d)	2.85	2.61(g)	3.42
F.C.2	4.76		3.93	3.94	4.62	4.21	4.89

Active and near Active Constraints

(a) Lower bound = .05, (b) Lower bound = 500, (c) Lower bound = 1000, (d) Lower bound = 2.5, (e) Upper bound = 63, (f) Upper bound = 74.8, (g) Lower bound = 2.6, (h) Lower bound = .04, (j) Lower bound = .10, (k) Upper bound = 100°

* The same as Cases 2(a) and (d) of Ref. 10

\+ The same as Case 1 in Ref. 10

5. Concluding Remarks

The feasibility of performing optimal wing structure designs at a preliminary design stage was studied, and both the equivalent plate formulation and the finite element formulation were found to be useful. For most of the examples run, dynamic constraints assumed important roles in the design procedure, thus indicating the wisdom of considering these constraints at the preliminary design stage. Supersonic flutter in low altitude flight becomes an especially critical condition.

A simplified wing configuration design was shown to be feasible and it was found that the choice of the objective function had strong effects on the optimal configuration. Additional study will be necessary to determine a more realistic objective function for combining weight and drag, but the trends are clearly shown in the results.

Detailed material distribution design using the more precise structural analysis of the finite element method was presented and was also shown to be feasible.

In both phases of design, computation time required for one complete design ranged from 0.6 to 1.5 hours on a UNIVAC 1108 computer. This was achieved by taking advantage of special structures of the problems and by utilizing human judgement at various stages during run time. Even considered as a subsystem to be used in an integrated design system, these requirements on computational time of approximately one hour may be acceptable.

While it may be desirable to completely automate the entire procedure of the design, especially inside each subsystem, it is recognized that a certain level of man-machine communication can save a great deal of programming effort and computation time.

References

1. Ashley, H., McIntosh, S. C., Weatherill, W. H., "Optimization under Aeroelastic Constraints", AGARD Conference Proc., No. 36, on Symposium on Structural Optimization, October 1970.

2. Turner, M. J., "Design of Minimum Mass Structures with Specified Natural Frequencies", AIAA J., Vol. 5, No. 3, March 1967.

3. Zarghamee, M. S., "Optimal Frequency of Structures", AIAA J., Vol. 6, No. 4, April 1968.

4. Rubin, C. P., "Dynamic Optimization of Complex Structures", Proc. AIAA/ASME 10th Structures, Structural Dynamics and Materials Conference, New Orleans, La., April 1969.

5. Fox, R. L., Kapoor, M. D., "Rates of Changes of Eigenvalues and Eigenvectors", AIAA J., Vol. 6, No. 12, December 1968.

6. Schmit, L. A., Thornton, W. A., "Synthesis of an Airfoil at Supersonic Mach Number", NASA CR-144, January 1965.

7. Turner, M. J. "Optimization of Structures to Satisfy Flutter Requirements", Proc. AIAA/ASME 10th Structures, Structural Dynamics and Materials Conference, New Orleans, Louisiana, April 1969.

8. Stroud, W. J., Dexter, C. B., Stein, M., "Automatic Preliminary Design of Simplified Wing Structures to Satisfy Strength and Flutter Requirements", Langley Working Paper 961, May 1971.

9. Miura, H., "An Optimal Configuration Design of Lifting Surface Type Structures under Dynamic Constraints", Ph.D. Thesis, Case Western Reserve University, January 1972. Also Report No. 48, Division of Solid Mechanics, Structures and Mechanical Design, Case Western Reserve University, October 1971.

10. Rao, S. S., "Automated Optimum Design of Aircraft Wings to Satisfy Strenght, Stability, Frequency and Flutter Requirements". Ph.D. Thesis, Case Western Reserve University, January 1972. Also Report No. 49, Division of Solid Mechanics, Structures and Mechanical Design, Case Western Reserve University, October 1971.

11. Archer, John S., "Consistent Mass Matrices for Distributed Mass System", J. Structural Division, Proc. ASCE, Vol. 89, No. ST-4, Part 1, August 1963.

12. Ashley, H., Zartarian, G., "Piston Theory - A New Aerodynamic Tool for the Aeroelasticial", J. of the Aeronautical Sciences, Vol. 23, No. 12, December 1956.

13. Giles, G. L., "A Procedure for Automating Aircraft Wing Structural Design", Proc. 5th Conference on Electronic Computation, ASCE Purdue Univ. August 1970.

14. Mills, W. R., "Procedures for Including Temperature Effects in Structural Analysis of Elastic Wings - Part I", WADC TR 57-754, 1958.

15. Gallagher, R. H., Rattinger, I., Archer, J. S., "A Correlation Study of Methods of Matrix Structural Analysis", The Macmillan Co., New York, 1964.

16. Tinawi, R. A., "A Study of Various Idealizations for Wing Structures and Numerical Procedures Involved Using Matrix Methods", AIAA Structures, Structural Dynamics and Materials Conference, New Orleans, La., April 1969.

17. Flemming, M., "Practical Application of Finite Element Methods in the Design of Structures", Symposium on Structural Optimization, AGARD Conference Proc., No. 36, 1970.

18. Fletcher, R., Reeves, C. M., "Function Minimization by Conjugate Gradients", Computer J., Vol. 7, No. 2, February 1964.

19. Zoutendijk, G., "Method of Feasible Directions", Elsevier Publishing Co., Amsterdam, 1960.

20. Vanderplaats, G. N., "Automated Design of Elastic Trusses for Optimum Geometry", Ph.D. Thesis, Case Western Reserve University, June 1971. Also Report No. 44, Division of Solid Mechanics, Structures and Mechanical Design, Case Western Reserve

University, June 1971.

21. Fox, R. L., "Optimization Methods for Engineering Design", Addison Wesley, Reading, Mass., 1971.

22. Turner, M. J., Clough, R. W., Martin, H. C., Topp, L. J., "Stiffness and Deflection Analysis of Complex Structures", J. of the Aeronautical Sciences, Vol. 23, No. 9, September 1956.

23. Fletcher, R., Powell, M. J. D., "A Rapidly Convergent Descent Method for Minimization", Computer J., Vol. 6, No. 2, 1963.

24. Lasdon, L. S., Fox, R. L., Ratner, M. W., "An Efficient One-Dimensional Search Procedure for Barrier Functions", Report No. 46, Division of Solid Mechanics, Structures and Mechanical Design, Case Western Reserve University, September 1971.

AUTOMATED DESIGN OPTIMIZATION OF SUPERSONIC AIRPLANE WING STRUCTURES UNDER DYNAMIC CONSTRAINTS*

Richard L. Fox

Hirokazu Miura

Singiresu S. Rao

April 1972

(Revised October 1972)

* This paper is a revision of Paper No. 72-333 by the same title presented at the AIAA/ASME/SAE 13th Structures, Structural Dynamics and Materials Conference, San Antonio, Texas, April 10-12, 1972.

SYNOPTIC BACKUP DOCUMENT

This document is made publicly available through the NASA scientific and technical information system as a service to readers of the corresponding "Synoptic" which is scheduled for publication in the following (checked) technical journal of the American Institute of Aeronautics and Astronautics.

- ☐ AIAA Journal
- ☒ Journal of Aircraft, June 1973
- ☐ Journal of Spacecraft & Rockets
- ☐ Journal of Hydronautics

A Synoptic is a brief journal article that presents the key results of an investigation in text, tabular, and graphical form. It is neither a long abstract nor a condensation of a full length paper, but is written by the authors with the specific purpose of presenting essential information in an easily assimilated manner. It is editorially and technically reviewed for publication just as is any manuscript submission. The author must, however, also submit a full backup paper to aid the editors and reviewers in their evaluation of the synoptic. The backup paper, which may be an original manuscript or a research report, is not required to conform to AIAA manuscript rules.

For the benefit of readers of the Synoptic who may wish to refer to this backup document, it is made available in this microfiche (or facsimile) form without editorial or makeup changes.